



Organic Aerosols in the Presence of CO₂ in the Early Earth and Exoplanets: UV–Vis Refractive Indices of Oxidized Tholins

Liseth Gavilan, Laurent Broch, Nathalie Carrasco, Benjamin Fleury, Ludovic Vettier

► To cite this version:

Liseth Gavilan, Laurent Broch, Nathalie Carrasco, Benjamin Fleury, Ludovic Vettier. Organic Aerosols in the Presence of CO₂ in the Early Earth and Exoplanets: UV–Vis Refractive Indices of Oxidized Tholins. The Astrophysical journal letters, 2017, 848 (1), pp.L5. 10.3847/2041-8213/aa8cc4 . insu-01808648

HAL Id: insu-01808648

<https://insu.hal.science/insu-01808648>

Submitted on 5 Jun 2018

HAL is a multi-disciplinary open access archive for the deposit and dissemination of scientific research documents, whether they are published or not. The documents may come from teaching and research institutions in France or abroad, or from public or private research centers.

L'archive ouverte pluridisciplinaire **HAL**, est destinée au dépôt et à la diffusion de documents scientifiques de niveau recherche, publiés ou non, émanant des établissements d'enseignement et de recherche français ou étrangers, des laboratoires publics ou privés.

ORGANIC AEROSOLS IN THE PRESENCE OF CO₂ IN THE EARLY EARTH AND EXOPLANETS: UV-VIS-NIR REFRACTIVE INDICES OF OXIDIZED THOLINS

LISSETH GAVILAN,¹ LAURENT BROCH,² NATHALIE CARRASCO,¹ BENJAMIN FLEURY,³ AND LUDOVIC VETTIER¹

¹*LATMOS, Université Versailles St Quentin, UPMC Université Paris 06, CNRS, 11 blvd d'Alembert, 78280 Guyancourt, France*

²*LCP-A2MC, Institut Jean Barriol, Université de Lorraine, Metz, France*

³*Jet Propulsion Laboratory, California Institute of Technology, Pasadena, CA 91109, USA*

ABSTRACT

The goal of this experimental study is to investigate how the presence of atmospheric CO₂ affects the optical properties of organic photochemical aerosols. To this end, we add CO₂ to a N₂:CH₄ gas mixture used in a plasma typically used for Titan studies. We produce organic thin films (*tholins*) in plasmas where the CO₂ / CH₄ ratio is increased from 0 to 4. We measure these films via spectrometric ellipsometry in the ultraviolet, visible and near-infrared (270 nm to 2 μ m). The ellipsometry parameters are fitted with a Tauc-Lorentz model used for optically transparent materials, to obtain the thickness of the thin film, its optical band gap, and the refractive indices. According to this optical mode, oxidized organic aerosols are transparent in the visible up to the near ultraviolet ($k = 0$ from 900 - 400 nm), while the fully reduced organic aerosol absorbs in the visible as well as in the near UV ($k = 0$ from 900 - 500 nm). As the CO₂/CH₄ ratio is quadrupled, the position of the UV absorption resonance is shifted from ~ 177 nm to 264 nm, and its strength is also quadrupled: oxidized tholins absorb more efficiently in the middle UV with respect to the far UV for reduced tholins. Our laboratory wavelength-tabulated refractive indices provide further constraints to atmospheric models of the early Earth and Earth-like exoplanets including photochemical hazes formed under increasingly oxidizing conditions.

Keywords: Planets and satellites: atmospheres, fundamental parameters - Methods: laboratory: solid state - Techniques: spectroscopic

1. INTRODUCTION

The presence of CO_2 in planetary atmospheres can modify the production of photochemical aerosols. In the solar system, CO_2 is the dominant component in the atmospheres of Mars (95.97 %) and Venus (96.5 %). On Earth, substantial evidence points that life came into existence either near the end of the Hadean Eon (4.6 - 4 Myr) or early in the Archean Eon (4 - 2.5 Myr) releasing oxygen into the atmosphere (Kasting 1993). The atmosphere of the early Earth was N_2 dominated and models show that it could have included up to 3 - 10 % of CO_2 as well as CH_4 (Feulner 2012; von Paris et al. 2008). CO_2 is considered to be the dominant greenhouse gas offsetting the early Sun that could have kept the early Earth unfrozen, but it could also be removed from the atmosphere by the flow of carbon into the mantle (Sleep & Zahnle 2001).

It has been hypothesized that photochemistry in the early Earth's atmosphere could lead to formation of organic hazes (Haqq-Misra et al. 2008; Wolf & Toon 2010). Depending on their optical properties, hazes could impact planetary habitability via UV shielding and surface cooling (Pavlov et al. 2001). Paleoclimate models that include organic hazes (e.g. Charnay et al. 2013; Arney et al. 2016) usually incorporate laboratory optical constants of tholins produced under Titan's reducing conditions. Such models typically refer to the seminal work by Khare et al. (1984). Laboratory optical properties of oxidized organic aerosols are needed to refine models of the Archean Earth but also of exoplanet atmospheres. Although CO_2 is considered a minor carrier of carbon in exoplanetary atmospheres (Heng & Lyons 2016), its presence could greatly affect the formation and optical properties of photochemical hazes in Earth-like exoplanets (Arney et al. 2017).

The aim of this work is to experimentally simulate the composition of increasingly oxidizing atmospheres to understand the impact of CO_2 in the optical properties of the generated organic aerosols. Although previous works have investigated the impact of CO_2 on the aerosol yield and chemical composition (Trainer et al. 2006; Fleury et al. 2014) we investigate the effect of an increasing CO_2 concentration on the optical properties of the plasma-produced solids.

2. METHODS

Tholins, complex nitrogenated organic solids, were produced using the PAMPRE setup, a low pressure (0.95 mbar) radiofrequency (RF) plasma reactor (Szopa et al. 2006). This setup allows the simulation of the complex organic chemistry initiated by VUV solar photons in the ionosphere of the early Earth and Titan (Fleury

et al. 2014). A 13.56 MHz RF power source tuned at 30 W generates a capacitively coupled plasma (CCP) fed by a gas mixture. We start by producing a plasma with a gas mixture simulating the reducing composition of Titan's atmosphere, i.e. $\text{N}_2:\text{CH}_4$ at 95:5 ratios (e.g. Sciamma-O'Brien et al. 2012). We then prepare tholins at increasingly oxidizing conditions by adding CO_2 to this gas mixture. A first mixture of $\text{N}_2:\text{CO}_2:\text{CH}_4$ at 90:5:5 ratios keeps the same CH_4 concentration as the reference tholin and a ratio of CO_2/CH_4 of 1. A second condition of 95:2.5:2.5 keeps the same CO_2/CH_4 of 1 while increasing the concentration of N_2 . A third gas mixture of 90:2:8 ratios allows us to test a most oxidizing scenario where $\text{CO}_2/\text{CH}_4 = 4$.

The plasma is produced within a vertical cylindrical cage. Bare silicon (10×10 mm) and MgF_2 windows (20 mm diameter) are placed on the bottom electrode, but we only report here the results obtained on the films deposited on the Si substrates. Spectroscopy of the films deposited on the MgF_2 windows will be the main subject of a forthcoming study. The plasma is turned on until a thin film is deposited for the durations listed in Table 1. We note from these values that the thin film yield is drastically quenched as the CO_2/CH_4 ratio increases, consistent with previous studies (Trainer et al. 2006; Fleury et al. 2014). Hicks et al. (2016) recently showed that in such gas mixtures CH_4 contributes 70-100% of carbon in the aerosol, while CO_2 contributes approximately 10% of oxygen in the aerosol.

3. ANALYSIS

3.1. UV-Visible ellipsometry

Ellipsometric measurements are performed on the tholin films prepared in plasmas with and without CO_2 . In spectroscopic ellipsometry (SE) light is elliptically polarized upon reflection from a sample. The ratio of the incident to the reflected light amplitude $\tan(\Psi)$ and the relative phase change for the p- and s- polarized light components (Δ) result from the interaction between the light with both the organic film and the Si substrate. SE is a robust method for the optical characterization of thin films because it measures two physical magnitudes at each wavelength.

These measurements are done with an UVISEL ellipsometer (Horiba) located at the LCP-A2MC laboratory of the Institut Jean Barriol (Université de Lorraine). This instrument allows us to measure our samples from the ultraviolet to the near-infrared (**270 nm - 2030 nm**) thanks to a 150 W Xenon light source. Two incidence angles are used in these measurements: 70° illuminating an ellipsoidal spot of 2 mm × 4.85 mm on the film, and 60° illuminating an ellipsoidal spot of 2 mm ×

Table 1. Fitted parameters for a Tauc-Lorentz oscillator describing tholins thin films.

N ₂ :CO ₂ :CH ₄ duration ^a	χ ²	Thickness [nm]	E _g [eV]	A [eV]	C [eV]	E _o [eV]	ε _r (∞)	SiO ₂ [nm]	SiO ₂ +Tholin [nm]
95:0:5 [3']	0.07	36.02 ± 0.03	2.48 ± 0.04	10.92 ± 0.29	4.39 ± 0.10	6.16 ± 0.06	2.10 ± 0.01		
90:5:5 [20']	0.93	78.80 ± 0.05	2.54 ± 0.02	17.57 ± 0.69	5.43 ± 0.23	7.63 ± 0.13	1.79 ± 0.03		
95:2.5:2.5 [15']	0.67	79.04 ± 0.04	2.53 ± 0.01	17.24 ± 0.42	4.88 ± 0.12	6.90 ± 0.06	1.87 ± 0.01		
90:8:2 [480']	0.32 ^b	26.56 ± 0.38	3.06 ± 0.04	39.02 ± 2.56	3.26 ± 0.07	4.71 ± 0.05	2.33 ± 0.02	8.44 ± 0.42	
	0.30 ^c	10.49 ± 0.45	2.97 ± 0.04	48.04 ± 4.59	2.96 ± 0.06	4.71 ± 0.03	2.37 ± 0.04		24.38

^aThe duration refers to the time the plasma was kept on at 30 W

^bmodel 2: Si+SiO₂+Tholin

^cmodel 3: Si+(44.2 % SiO₂+Tholin, 55.8 % Tholin)+Tholin

4 mm. The reflected light is integrated over at least half the film area. For the near infrared range (880 - 2100 nm) an InGaAs detector is used.

3.1.1. Tauc-Lorentz model

A dispersion model is required to fit the ellipsometric parameters Ψ and Δ for each wavelength. This is done via the *DeltaPsi2* software platform. For all samples the organic layer is fitted by a Tauc-Lorentz oscillator, shown to effectively describe the optical properties of tholins in the UV-visible (Mahjoub et al. 2012). Jellison & Modine (1996) developed this model based on the Tauc joint density of states and the Lorentz oscillator. This oscillator is typically used to model absorbing materials, and an optically (visible) transparent material can be described as a sum of Lorentz oscillators in the UV. The Tauc-Lorentz model is a further refinement to the Lorentz oscillator and adapts well to amorphous materials with an absorption in the visible and/or ultra-violet such as dielectrics, semiconductors and polymers.

In this model, the imaginary part of the dielectric function is given by the product of the imaginary part of Tauc's dielectric function (Tauc et al. 1966) with a Lorentzian oscillator,

$$\varepsilon_{i,TL}(E) = \begin{cases} \frac{AE_oC(E - E_g)^2}{E(E^2 - E_o^2)^2 + C^2E^2}, & \text{for } E > E_g \\ 0, & \text{for } E \leq E_g \end{cases} \quad (1)$$

where E_g (in eV) is the optical band gap energy, which specifies at which energy the material becomes absorbing. E_o (in eV) is the energy position of the major absorption peak in the UV ($E_g < E_o$). A (in eV) is related to the strength of this absorption peak while C (in eV) is related to its broadening or damping. The fitted parameters are listed in Table 1.

The real part $\varepsilon_{r,TL}(E)$ of the dielectric function is derived from the expression of ε_i using the Kramers-

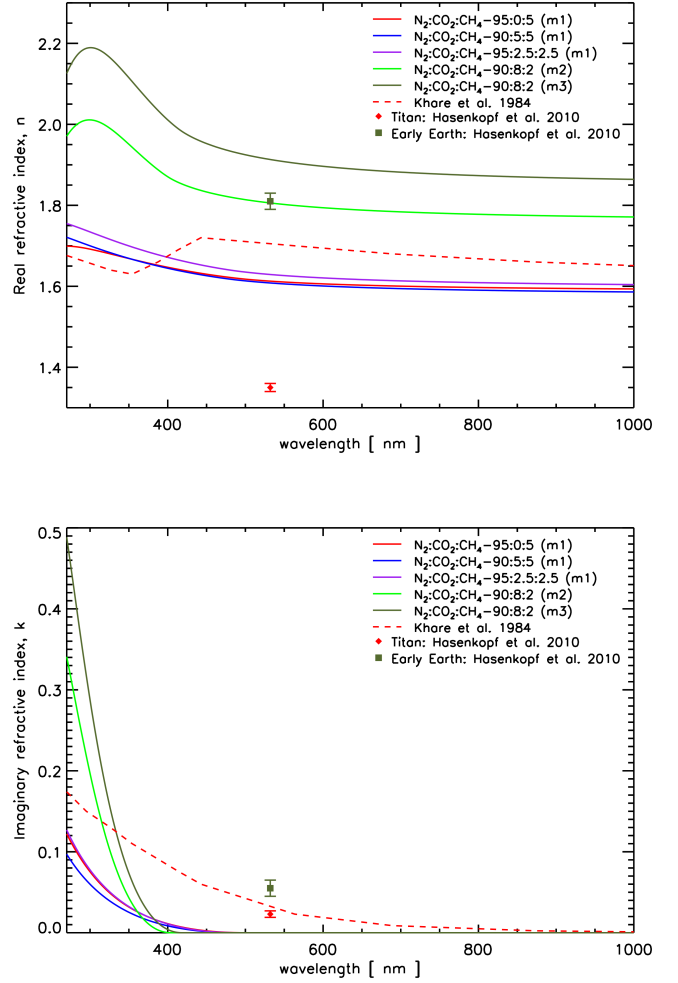


Figure 1. Refractive indices in the UV-Visible (270 nm - 2000 nm) for tholins prepared with different mixtures of N₂:CO₂:CH₄. As the CO₂/CH₄ ratio increases, the strength of the major UV absorption is significantly increased.

Kronig closure relations, so that,

$$\varepsilon_r(E) = \varepsilon_r(\infty) + \frac{2}{\pi} P \int_{E_g}^{\infty} \frac{\xi \cdot \varepsilon_i(\xi)}{\xi^2 - E^2} d\xi, \quad (2)$$

Table 2. UV-Visible-NIR refractive indices of tholins: 1) 95:0:5 (no CO₂, model 1), 2) 90:5:5 (CO₂/CH₄ = 1, model 1), 3) 90:8:2 (CO₂/CH₄ = 4, model 3).

λ [nm]	95/0/5		90/5/5		90/8/2	
	n	k	n	k	n	k
270	1.699	1.22E-01	1.721	9.70E-02	2.126	4.88E-01
282	1.698	1.01E-01	1.713	8.01E-02	2.168	4.06E-01
294	1.694	8.31E-02	1.704	6.60E-02	2.187	3.25E-01
306	1.689	6.82E-02	1.696	5.43E-02	2.188	2.52E-01
318	1.684	5.58E-02	1.688	4.45E-02	2.177	1.89E-01
330	1.678	4.54E-02	1.681	3.62E-02	2.157	1.37E-01
342	1.672	3.67E-02	1.673	2.93E-02	2.133	9.60E-02
354	1.667	2.94E-02	1.667	2.34E-02	2.106	6.37E-02
366	1.661	2.34E-02	1.660	1.85E-02	2.079	3.94E-02
378	1.656	1.83E-02	1.654	1.44E-02	2.054	2.19E-02
390	1.651	1.41E-02	1.649	1.09E-02	2.029	1.01E-02
402	1.646	1.07E-02	1.644	8.08E-03	2.008	3.12E-03
414	1.642	7.83E-03	1.639	5.76E-03	1.988	1.87E-04
426	1.637	5.54E-03	1.634	3.90E-03	1.974	0
438	1.634	3.72E-03	1.630	2.46E-03	1.962	0
450	1.630	2.32E-03	1.626	1.38E-03	1.953	0
462	1.626	1.28E-03	1.623	6.35E-04	1.944	0
474	1.623	5.75E-04	1.619	1.86E-04	1.937	0
486	1.620	1.58E-04	1.616	6.00E-06	1.931	0
498	1.618	3.00E-06	1.614	0	1.926	0
510	1.616	0	1.612	0	1.921	0
522	1.614	0	1.610	0	1.916	0
534	1.612	0	1.608	0	1.912	0
552	1.610	0	1.606	0	1.907	0
576	1.608	0	1.603	0	1.901	0
600	1.606	0	1.601	0	1.896	0
624	1.604	0	1.599	0	1.892	0
648	1.603	0	1.597	0	1.888	0
672	1.602	0	1.596	0	1.885	0
696	1.600	0	1.594	0	1.882	0
720	1.600	0	1.593	0	1.880	0
744	1.599	0	1.592	0	1.878	0
768	1.598	0	1.591	0	1.876	0
792	1.597	0	1.591	0	1.874	0
816	1.597	0	1.590	0	1.872	0
840	1.596	0	1.589	0	1.871	0
864	1.596	0	1.589	0	1.870	0
888	1.595	0	1.588	0	1.868	0
912	1.595	0	1.588	0	1.867	0
942	1.594	0	1.587	0	1.866	0
972	1.594	0	1.586	0	1.865	0
1002	1.593	0	1.586	0	1.864	0
1032	1.593	0	1.586	0	1.863	0
1068	1.593	0	1.585	0	1.862	0
1110	1.592	0	1.585	0	1.861	0
1152	1.592	0	1.584	0	1.860	0
1194	1.592	0	1.584	0	1.859	0
1242	1.591	0	1.583	0	1.859	0
1296	1.591	0	1.583	0	1.858	0
1350	1.591	0	1.583	0	1.857	0
1416	1.590	0	1.582	0	1.856	0
1482	1.590	0	1.582	0	1.856	0
1554	1.590	0	1.582	0	1.855	0
1638	1.590	0	1.581	0	1.854	0
1836	1.589	0	1.581	0	1.853	0
2030	1.589	0	1.581	0	1.853	0

where $\varepsilon_r(\infty)$ is the high frequency real dielectric constant, and P is the Cauchy principal value containing the residues of the integral at the poles on the lower half of the complex plane and along the real axis.

Because the ellipsometric parameters only slightly vary from 870 to 2000 nm, fitting is first done in the 270 - 870 nm region, optimizing the χ^2 in this range, and later used to calculate the optical constants over the entire range. To model the thin films described in Table 1, we use three models to optimize the ellipsometric fit for each type of sample. Model 1 (m1) consists of an Si substrate, covered by an organic thin film, and best describes the Titan tholin (95:0:5) and the low-oxidation tholin (90:5:5). To describe the most oxidized tholin we try a second model (m2), consisting of an Si substrate, covered by an SiO₂ thin layer, itself covered by an organic thin film. A CO₂/CH₄ = 4 plasma is able to oxidize the surface of the Si substrate generating silicon dioxide. A third model (m3) further refines this by generating a mixed layer of SiO₂ with the tholin. It consists of an Si substrate, a mixed layer consisting of the refracted indices of SiO₂ and the tholin, and a pure tholin layer. The m3 model was found to best fit the ellipsometric parameters of the most oxidized tholin.

Optimizing the number of layers and their mixing is necessary to best adjust the ellipsometric data. This is the case for the most oxidized tholin (90:8:2), for which the oxidizing plasma reacted with the Si substrate producing SiO₂. Such reactions could form a single SiO₂ layer but the improved fit with model (m3) seems to indicate that an intermediate material, a mixture of the tholin with SiO₂, best accounts for this surface reactivity. Since this reaction happens close to the surface, the top layer in this sample is fitted by a pure tholin. The choice of an Si substrate is justified since this single-side polished material is reflective (ideal for ellipsometry) and it simplifies the number of parameters used to model the organic and substrate layers. The modeled real and imaginary refractive indices obtained by the best χ^2 models are presented in Fig. 1. Their wavelength-dependent refractive indices are listed in Table 2.

As the CO₂/CH₄ ratio increases from 0 to 1, the optical gap E_g shifts from 500 nm to 488 nm (2.48 to 2.54 eV), and for CO₂/CH₄ = 4, the optical gap E_g value shifts to even shorter wavelengths, 400 nm (3 eV). This means that an oxidized organic aerosol is transparent in the visible up to the near ultraviolet ($k = 0$ from 900 - 400 nm), while a reduced organic aerosol absorbs in the visible as well as in the near UV ($k = 0$ from 900

- 500 nm). As the CO₂/CH₄ ratio is quadrupled, the position of the UV absorption resonance is shifted from ~177 nm to 264 nm and its strength is also quadrupled: oxidized tholins absorb more efficiently in the middle UV with respect to the far UV for reduced tholins.

In Fig. 1, we compared the refractive indices for oxidized and reduced tholins in this study to the optical constants from Khare et al. (1984) and Hasenkopf et al. (2010). In this latter work, Titan and early Earth organic haze aerosols analogs are measured using cavity ring-down aerosol extinction spectroscopy on freely-floating particles. Their Titan analog has a much smaller real refractive index, n , compared to our measurements for the fully reduced tholin (95:0:5) and to values in (Khare et al. 1984). In contrast, the real index value of their early Earth analog at 532 nm is close to ours. For the imaginary index, k , the 532 nm values in Hasenkopf et al. (2010) are larger than our modeled values, and are more similar to those found in Khare et al. (1984). McKay et al. (2001) pointed out that the sharp drop (k dropping as the power of 4) in absorption from 300 nm to 900 nm in a tholin spectra is essential for reproducing the shape of Titan’s geometric albedo. Neither our fully reduced tholin, nor the poly-HCN tholins used in (Khare et al. 1984) present this sharp drop. Although our reduced tholin is not an ideal Titan analog, it has allowed us to perform a comparative study (increasing the CO₂/CH₄ ratio) with the same instrumental setup, and to compare the optical properties of similar organic solids by leaving oxidation as the single free parameter.

4. ASTROPHYSICAL IMPLICATIONS

Our experiments show that a varying atmospheric CO₂/CH₄ ratio can significantly modify the optical properties of organic aerosols. Tholins produced under an oxidizing plasma present a larger band gap than tholins produced in a reduced plasma, i.e. their absorption begins in the UV rather than the visible range. Furthermore, oxidized tholins are much better absorbers in the UV than reduced tholins (as much as four times more absorbing, at least up to the measured energy of 4.59 eV).

The strong UV absorption of oxidized tholins is particularly relevant to the early Earth when we consider the blue-shifted spectrum of a young Sun (Cnossen et al. 2007). Solar far-ultraviolet (FUV) emission was about

twice the present value 2.5 Gyr ago and about 4 times the present value 3.5 Gyr ago (Guinan et al. 2003). Oxidized aerosols could have contributed to UV shielding from the young Sun prior to the onset of much more oxidizing conditions (CO₂/CH₄ > 4), which mitigates the formation of photochemical hazes.

This study provides, for the first time, laboratory wavelength-dependent refractive indices of oxidized organic aerosols in the UV-Visible-NIR range at increasing degrees of oxidation. Such indices can be used to refine radiative transfer models of increasingly oxidizing planetary atmospheres including photochemical hazes. These can be further incorporated to atmospheric models of the early Earth but also of Earth-like exoplanets (e.g. Forget & Leconte 2014).

5. ACKNOWLEDGEMENTS

We thank Dr. Pavel Bulkin (LPICM, Ecole Polytechnique) for his help with the preliminary measurements. N.C. and L.G. thank the European Research Council for funding via the ERC *PrimChem* project (grant agreement No. 636829.)

REFERENCES

- Arney, G., Domagal-Goldman, S. D., Meadows, V. S., et al. 2016, *Astrobiology*, 16, 873
- Arney, G. N., Meadows, V. S., Domagal-Goldman, S. D., et al. 2017, *ApJ*, 836, 49
- Charnay, B., Forget, F., Wordsworth, R., et al. 2013, *Journal of Geophysical Research (Atmospheres)*, 118, 10
- Crossen, I., Sanz-Forcada, J., Favata, F., et al. 2007, *Journal of Geophysical Research (Planets)*, 112, E02008
- Feulner, G. 2012, *Reviews of Geophysics*, 50, RG2006
- Fleury, B., Carrasco, N., Gautier, T., et al. 2014, *Icarus*, 238, 221
- Forget, F., & Leconte, J. 2014, *Philosophical Transactions of the Royal Society of London Series A*, 372, 20130084
- Guinan, E. F., Ribas, I., & Harper, G. M. 2003, *ApJ*, 594, 561
- Haqq-Misra, J. D., Domagal-Goldman, S. D., Kasting, P. J., & Kasting, J. F. 2008, *Astrobiology*, 8, 1127
- Hasenkopf, C. A., Beaver, M. R., Trainer, M. G., et al. 2010, *Icarus*, 207, 903
- Heng, K., & Lyons, J. R. 2016, *ApJ*, 817, 149
- Hicks, R. K., Day, D. A., Jimenez, J. L., & Tolbert, M. A. 2016, *Astrobiology*, 16, 822
- Jellison, Jr., G. E., & Modine, F. A. 1996, *Applied Physics Letters*, 69, 371
- Kasting, J. F. 1993, *Science*, 259, 920
- Khare, B. N., Sagan, C., Arakawa, E. T., et al. 1984, *Icarus*, 60, 127
- Mahjoub, A., Carrasco, N., Dahoo, P.-R., et al. 2012, *Icarus*, 221, 670
- McKay, C. P., Coustenis, A., Samuelson, R. E., et al. 2001, *Planet. Space Sci.*, 49, 79
- Pavlov, A. A., Brown, L. L., & Kasting, J. F. 2001, *J. Geophys. Res.*, 106, 23267
- Sciamma-O'Brien, E., Dahoo, P.-R., Hadamcik, E., et al. 2012, *Icarus*, 218, 356
- Sleep, N. H., & Zahnle, K. 2001, *Journal of Geophysical Research*, 106, 1373
- Szopa, C., Cernogora, G., Boufendi, L., Correia, J. J., & Coll, P. 2006, *Planetary and Space Science*, 54, 394
- Tauc, J., Grigorovici, R., & Vancu, A. 1966, *Physica Status Solidi B-basic Solid State Physics*, 15, 627
- Trainer, M. G., Pavlov, A. A., Dewitt, H. L., et al. 2006, *Proceedings of the National Academy of Science*, 103, 18035
- von Paris, P., Rauer, H., Lee Grenfell, J., et al. 2008, *Planetary and Space Science*, 56, 1244
- Wolf, E. T., & Toon, O. B. 2010, *Science*, 328, 1266